International Journal of Refractory Metals and Hard Materials 126 (2025) 106954

Contents lists available at ScienceDirect

International Journal of Refractory Metals and Hard Materials

journal homepage: www.elsevier.com/locate/IJRMHM

Effect of chromium doping on the grain boundary character of WC-Co

Max Emmanuel [a], Zhuoqi Lucas Li [a,*], Harry Heptinstall [a,*], Oriol Gavalda-Diaz [a], Rachid M'saoubi [b], Tomas Persson [b], Susanne Norgren [c], Thomas Benjamin Britton [a,d], Finn Giuliani [a], Katharina Marquardt [a,e]

[a] Department of Materials, Imperial College London, London SW7 2AZ, UK
[b] R&D Material and Technology Development, Seco Tools AB, SE73782, Fagersta & Division of Production and Materials Engineering, Lund University, Ole Römers väg 1, 22100 Lund, Sweden
[c] Stockholm & Division of Production and Materials Engineering, Lund Technical University, Sandvik R&D, Lerkrogsv. 13, SE12680, Sweden
[d] Department of Materials Engineering, The University of British Columbia, Vancouver, B.C. V6T 1Z4, Canada
[e] Department of Materials, University of Oxford, Oxford OX2 6NN, UK

ARTICLE INFO

Keywords:
Electron backscatter diffraction (EBSD)
Grain boundary character distribution
Hard metal
Cemented carbide

ABSTRACT

The life of cutting tool inserts is critically important for efficient machining, reducing manufacturing cost, embedded energy, and enabling more complex parts to be machined. For these applications, cemented carbide (WC-Co) materials are a prime candidate. The performance of these materials can be limited by early fracture, typically via an intergranular fracture path with respect to carbide grains. This motivates further studies to understand the character of the grain boundary network so that grain boundary engineering (GBE) of WC-Co tools can be used to improve tool life and performance. In this work, we have used Rohrer et al.'s five-parameter grain boundary character distribution (GBCD) analysis to examine the grain boundary network of WC-10wt%Co and WC-10wt%Co-1wt%Cr samples (Rohrer et al., 2004a [1]). It was found that the measured area fraction of the Σ2 boundaries was comparable to the values reported in the literature despite the relatively larger grain sizes (~14 μm) and higher cobalt contents. The result suggests that chromium doping increases the area fraction of Σ2 boundaries from 12.8 % to 14.8 %. It is proposed that this is a consequence of altering the Σ2 boundary energy, as associated with adding chromium.

1. Introduction

Cemented carbide is an engineering material for parts that are required to withstand wear and exhibit high toughness. The microstructure of this material is a composite containing hard carbide grains (e.g., WC) contained within a soft ductile matrix from the iron group (Co, Fe or Ni). The former provides high hardness while the latter gives a high toughness.

Cemented carbide is a rapidly growing market with a year-on-year increase in its production. The global WC-Co market currently evaluated at US$18.16 billion is expected to rise to US$26.24 billion by 2028 with a compound annual growth rate (CAGR) of 5.4 % over the same period [2]. Increased demand in multiple applications including the aforementioned ones is the driving force for the WC-Co market growth. Thus, the interest in studying WC-Co.

Typically for cutting tool applications, WC-Co is produced via powder metallurgy processes. In brief, pure WO_2/WO_3 with a controlled grain size is produced from an ore and then carburized to form a WC powder. The WC powder particles inherit the grain size from the WO_2/WO_3 powder. The WC particles are blended to form a controlled mix of particles sizes, dictated by the products requirements, and mixed with Co metal (and other minor additives). This mixture is blended with alcohol, and ball milled. The wet product is dried, and powder compressed into moulds, prior to a final sintering step.

The resulting WC cutting tools are used in a wide array of applications such as machining of materials, chip-less forming, mining, industrial nozzles and wear parts. This is possible due to varying the WC grain size, binder content or binder composition during manufacture.

The WC grain boundary network in WC-Co is vital for mechanical properties and lifetimes of WC-Co components. Material toughness is related to energy dissipation, which in turn is dependent upon the crack path. Hence, gaining knowledge of the WC grain and phase boundary

* Corresponding authors.
E-mail addresses: zhuoqi.li17@imperial.ac.uk (Z.L. Li), h.heptinstall23@imperial.ac.uk (H. Heptinstall).

https://doi.org/10.1016/j.ijrmhm.2024.106954
Received 31 August 2024; Received in revised form 1 November 2024; Accepted 4 November 2024
Available online 7 November 2024

network is valuable. Particularly, because more than 50 % of the fracture path in WC-Co propagates via WC grain and phase boundaries at low cobalt contents, typical for most commercial grades [3]. Understanding the WC grain boundary network can inform the manufacturing of WC-Co tools with superior lifetimes and performance using grain boundary engineering (GBE).

There are two possible avenues for studying the grain boundary network. First, the properties of an established network can be measured, e.g., via micromechanical testing (e.g., fracture tests) at grain boundaries. Alternatively, the grain boundary population variation resulting from different chemistries and processing routes can be assessed. Here, we focus on the latter method and characterise the grain boundary population as a function of chemistry.

Microscopic grain boundary character, or its full geometry, is defined by five independent parameters [4]. Three parameters define the misorientation between grains that share any given boundary (Δg) and two that specify the orientation of the boundary plane normal ($\boldsymbol{n}$) [4]. The Δg can easily be determined from electron backscattered diffraction (EBSD). Direct access to $\boldsymbol{n}$ is a difficult task. This is because grain boundaries appear as line traces on planar sections of a sample. To define the plane normal, the grain boundary trace and the inclination of the plane marked by the trace are required. Therefore, only the trace of the grain boundary plane in the surface section is obtainable. This means that 2D EBSD can recover four of the five parameters to describe each grain boundary.

Various microscopy-based methods have been explored to investigate the fifth parameter, relating to the component of the boundary trace subsurface. For instance, optical microscopes were used to examine the grain boundary planes in thin samples, while crystal orientations were identified by analysing the images using computer-integrated polarisation microscopy (CIP) [5]. However, sample thin-sectioning is essential, and for samples with small grains, a substantial number of observations is needed [1]. Serial sectioning combined with EBSD provides accurate measurements of both boundary plane orientation and crystal orientation [6,7]; however, this method requires removing a thin layer from the sample surface (e.g., with a Ga-focussed ion beam (FIB), Xe plasma FIB, or mechanical sectioning), making it a destructive technique. In this paper, boundary shapes and distributions are studied via an indirect method to measure the fifth parameter using stereology and 2D EBSD maps. This approach follows Rohrer et al.'s five-parameter grain boundary character distribution (GBCD) analysis for the statistical analysis of two-dimensional EBSD data [1].

Processing and microstructure control can change the grain boundary network and our understanding of the grain boundary network is founded upon grain boundaries in their equilibrium energy state. However, grain boundaries are usually in metastable energy states related to being constrained by other grains growing, non-equilibrium grain growth (e.g. dendrites), material processing and external dynamic perturbations (e.g., plastic deformation and radiation damage). This is important as grain boundary energy dictates the grain boundary network, affecting material properties. Han et al. [8] have shown that multiple grain boundary states are possible especially for non-special boundaries. Given that non-special boundaries account for most of the boundaries in the grain boundary network and they have more grain boundary states, it is worth investigating the distribution of all possible grain boundaries in the material. Thus, the interest in using GBCD to study WC-Co.

Several studies have been conducted to examine the effect of microstructural parameters, processing conditions and deformation on the GBCD of WC-Co. Studies by Kim et al. [9] and Yuan et al. [10,11] have investigated the effect of WC grain size and cobalt content on the WC grain boundary distributions. Kim et al.'s work concluded that boundary populations did not vary with grain size and cobalt content, instead suggesting that the grain boundary energy anisotropy caused the change in the boundary populations. Meanwhile the two studies by Yuan et al. [10,11] conducted later affirmed that grain size and cobalt content affected grain boundary populations, specifically the Σ2 and Σ13 boundaries (90°/[10$\bar{1}$0] and 30°/[0001] in CSL notation, respectively). This was reflected as a reduction of Σ2 and Σ13 boundaries with increasing grain size or cobalt content. The authors studied these boundaries specifically as they are the most abundant WC/WC boundaries within WC-Co. Another study by Yuan et al. investigated the effect of alternative binders on GBCD of WC-Co for samples with similar grain sizes [12]. They conclude that the population of Σ2 boundaries increased with nickel as a binder instead of cobalt. The densification mechanism is another factor that influences Σ2 boundary population. This was shown in another work by Yuan et al. where it was found that spark plasma sintering (SPS) produced three times the area of Σ2 boundaries compared to use of sintering in hot isostatic press (sinter-HIP) [13]. The effect of plastic deformation on the distribution of the Σ2 boundaries have been studied in the literature revealing that the area fraction of Σ2 boundaries dropped with increasing plastic deformation.

The addition of dopants is likely to alter the boundary chemistry within a given sample. This is likely to change the boundary energy for boundaries of different character, and therefore the frequency of occurrence within the GBCD. In essence, as grain boundary energy increases, their relative fraction within the microstructure drops, provided the microstructure can relax during annealing processing. This is an important aspect of so called 'grain boundary engineering' and the effect of doping on GBCD has been investigated for materials such as MgO [14], Al_2O_3 [15] and SiC [16] and significant changes in grain boundary populations have been recorded. In the case of WC-Co, the effect of adding vanadium carbide (VC) has been investigated. It was found that the area fraction of Σ2 boundaries increased when doping with VC [17]. This change was hypothesised to be a result of the finer WC grain sizes and increased carbide contiguity in the doped sample.

The here presented study aims to meet three main objectives:

(1) To examine the important effect of chromium doping on the GBCD between a standard (WC-10wt%Co) and chromium doped sample (WC-10wt%Co-1wt%Cr).
(2) To measure and compare the area fractions for the most abundant boundary types (Σ2) to values reported in the literature.
(3) To link the observed abundance of specific grain boundaries to previous fracture toughness measured via double cantilever beam fracture testing [18].

2. Materials and methods

2.1. Sample preparation

The WC-Co polycrystalline samples used for this work were prepared by Susanne Norgren from Sandvik Hardmaterials (Stockholm, Sweden) and Lund Technical University. The polycrystalline samples were produced by conventional powder metallurgy means. Firstly, pure WC and Co powders were mixed by milling in ethanol-10 %H_2O. An extra coarse WC powder of 7 μm Fisher Sub Sieve grain size (FSSS) from Wolfram Bergbau und Hütten AG, Co from Freeport Cobalt and polyethylene glycol as pressing agent were used in the milling stage. The powder mixture was milled for 4 h inside a WC-lined 0.25 l rotating mill. The coarse WC powder and brief milling time made large WC grain formation possible. Thereafter, the powder mixture was tray dried at 40 °C in a N_2 atmosphere. Afterwards, the powder mixture was uniaxially pressed into a rectilinear (SNUN) geometry. The green bodies were placed in an H_2 atmosphere at 450 °C for debinding. Finally, the resulting green bodies were sintered at 1500 °C in controlled vacuum for an hour. A second batch of samples was produced in an analogy to the process detailed above, yet chromium powder was added during the milling stage. The processing for both samples was identical. A larger starting WC powder particle size coupled with a milling process that was more akin to mixing than milling meant the effect of grain growth inhibition effect of chromium was not observed. Thus, the finally sintered standard

(13.6 μm) and chromium doped (13.8 μm) samples have similar grain sizes, despite the grain growth-inhibiting effect of the chromium doping. The grain sizes were measured by the linear intercept method.

Once produced, samples were cut into 10x5x5 mm^3 size pieces with a Buehler Isomet 5000 Linear Precision Saw. A Beuhler EcoMetTM 250 Grinder-Polisher was then used to ground and polish the samples. Further finer polishing was achieved by broad ion beam milling the sample surface using a Gatan PECS II. The operation conditions for this step were 6 keV for 1.5 h and then 2 keV for 30 min at room temperature with the ion guns firing the beam at a glancing angle of 2° with respect to the horizontal.

2.2. EBSD data acquisition

EBSD data were acquired with a Bruker e-FlashHR detector inside a FEI Quanta 650 FEG-ESEM microscope. From the standard and doped WC-Co samples nine large maps of 830 × 550 μm^2 were acquired with a step size of 0.4 μm in a square grid. The acceleration voltage was set to 20 kV with an aperture size of 50 μm, an exposure time of 10 ms, a working distance of 15 mm, a sample-detector distance of approximately 15 mm and a detector tilt of 9°. EBSPs were recorded at a resolution of 200 × 150 pixels and analysed using the Bruker indexing algorithm. This resulted in indexing percentages of ~99 %.

2.3. EBSD data processing

EBSD data were processed via the EDAX OIM v8 Analysis™ software.

First the collected data, exemplified in Fig. 1, were exported as a .ctf from within the Bruker Esprit software before being imported into the OIM software. To address the difference in conventions for a non-cubic unit cell, the EBSD data was rotated by 30° for a hexagonal crystal structure with respect to the basis to account for the differences between the EDAX and Bruker data collection conventions.

Next, data clean-up was used to remove misindexed points so that the GBCD could be measured properly. First, grains and inclusions smaller than 200 and 100 pixels, respectively, were removed. Grains and inclusions were defined as being composed of multiple rows. Afterwards a grain dilation algorithm was applied limited to one dilation iteration, which changed 2–3 % of total data points. The cleaned data were then converted from the acquired square grid to a hexagonal sampling grid. The hexagonal sampling grid is attractive as it reduces 'locking' of features within the grain boundary network as associated with the sampling grid's horizontal, vertical, and diagonal grid lines.

The grain boundary traces are reconstructed first connecting triple junctions as nodes. The connecting boundary lines between the nodes are compared to the measured grain boundary network, and extra nodes are added where there is a deviation from the reconstructed boundary segment and the measured boundary segment and the maximum spatial deviation is greater than twice the step size. The resulting grain boundary traces are displayed in Fig. 1d.

Once the boundaries were reconstructed, the reconstructed WC boundary segments were extracted from each of the maps in the form of .txt files. These files contain information about the boundaries such as disorientation angles, grain boundary trace angles and grain boundary lengths. The disorientation angle represents the misorientation with the minimum rotation angle among all symmetrically equivalent misorientations that lie within the fundamental zone [19]. The nine boundary segment files for each of the samples were combined to produce one file containing all segments for each sample. The segments were sorted to include only WC/WC boundary segments. Thus segments related to the cobalt phase or a non-indexed data point were removed, identified by their Euler angles being trice zero Euler. Thus four grain boundary segment subsets were obtained: two for all possible WC boundary segments and two for WC/WC boundary segments for each sample. These segments were analysed using the full domain stereology codes written by Gregory S. Rohrer (CMU, Pittsburgh, PA, USA) in Fortran to plot disorientation distributions, axis-angle charts and GBCD plots [1].

3. Results

3.1. Disorientation distributions

The disorientation distributions were plotted for the disorientation angles between 0°-100° (Fig. 2). Disorientation distributions for both files are shown below. Deviating from the random disorientation distribution for hexagonal crystal systems is one peak at 90°, regardless of sample type. The 90° disorientation corresponds to Σ2 grain boundaries,

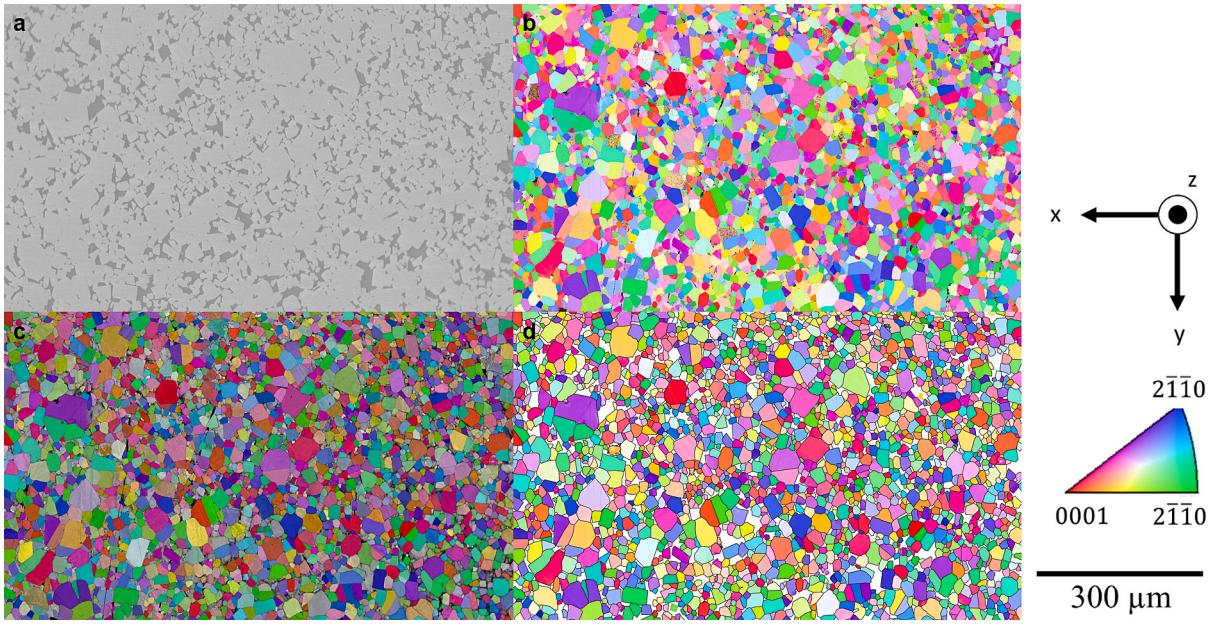

Fig. 1. (a) SEM image of a region from a WC-10wt%Co sample surface. Illustrations of the same region depicting (b) uncleaned IPF-Z map (c) cleaned IPF-Z map overlayed over image quality and (d) IPF-Z map with reconstructed boundaries after clean-up.

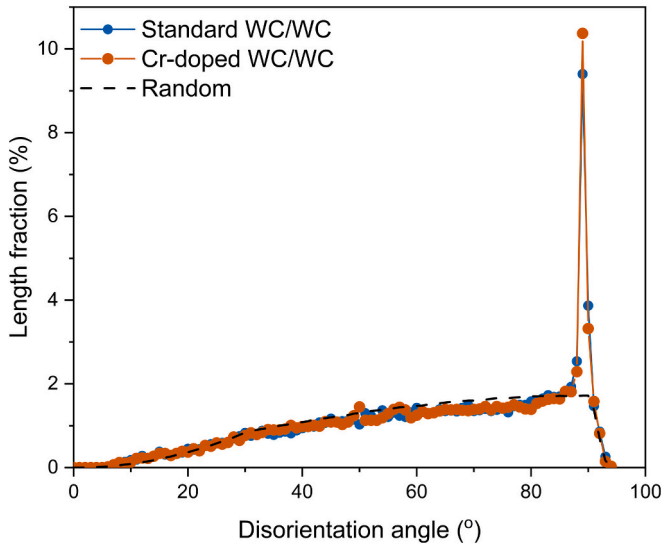

Fig. 2. Disorientation angle distribution for the two WC segment files: WC/WC files for the WC-10wt%Co and WC-10wt%Co-1wt%Cr samples. The random distribution for the WC boundaries is also included in the plot. Misorientation is the equivalent orientation differences between two grains while disorientation is used to describe the smallest of rotation angles among equivalent rotations relating two grains.

the size of the peaks indicates the population measured in boundary length fraction. Chromium addition increases the boundary length fractions for boundaries corresponding to the 90° disorientation peak as compared to the undoped sample. Notably, we did not observe a 30° disorientation, which in previous publications was observed and attributed to Σ13 grain boundaries [11,20]. The absence of a 30° disorientation peak agrees with the work of Li et al. [21].

Notably, when we did not follow a careful data cleaning regime, as discussed in Marquardt et al. [19,22] we observed a 30° disorientation peak. We were able to link this peak to pseudo-symmetric misindexing and describe the evaluation procedure in the supplementary material and **Fig. S1**.

3.2. Axis-angle distributions

Once the most dominant disorientation angle (90°) was found from the disorientation distributions, axis-angle distributions were plotted for the identified angle. This was done to determine the most frequent misorientation axis for the dominant disorientation angles. But most importantly, this step is vital for determining the area fraction of the Σ2 boundary. Axis-angle charts are given for the 90° disorientation in Fig. 3. The most abundant axis for the 90° disorientation was found to be $[10\bar{1}0]$. This in turn corresponds to the misorientations that define the Σ2 boundary.

3.3. Grain boundary character distributions

Once the misorientations were determined, GBCDs were plotted for the 90°/$[10\bar{1}0]$ boundaries. The GBCDs plotted are provided in Fig. 4. GBCD of the 90°/$[10\bar{1}0]$ boundaries regardless of the segment file show that the $\{10\bar{1}0\}$ planes (Σ2 twist) were the most abundant boundary habit planes with the MRD for the $\{11\bar{2}0\}$ and $\{0001\}$ planes (Σ2 tilt) being close to unity shows that the tilt variant does not occur more frequently than expected in a random distribution. The twist variant, however, is the most abundant boundary type in Σ2 boundaries.

The Σ2 area fractions were then calculated. This was performed in the following manner for each of the segment files. First the length fraction of the boundaries corresponding to the 90° peaks were measured. This was followed by recording the MRD attributed for the $[10\bar{1}0]$ axis from a fundamental zone in the 90° axis-angle distribution. Afterwards, the MRD attributed for the $\{10\bar{1}0\}$ planes were recorded within a fundamental zone. Then these three values were multiplied and divided by the number of bins within each of the fundamental zones of the axis-angle chart and GBCD plot. This is 54 bins in each of the cases. Σ2 area fractions determined for each of the four-segment files are presented in Table 1, which shows the increase in the area fraction of Σ2 boundaries from the standard (12.8 %) to chromium doped (14.8 %) WC-Co samples.

4. Discussion

The area fraction of the Σ2 boundaries measured for the standard sample is comparable to the values reported for other WC-Co samples in the literature. Table 2 provides the experimental parameters used in those studies.

The fractions of the Σ2 boundaries measured in the current work are comparable to the ones reported in prior work shown in Table 2**.** This is consistent with the findings of Kim et al., despite the differences in grain sizes and cobalt content [9].

Studies on the effect of GBCD of WC boundaries due to doping of WC-Co are lacking in the literature. A work by Liu et al. has examined the effect of doping WC-Co with another grain growth inhibitor in vanadium [17]. The authors found that the addition of 1 wt% VC resulted in the area fraction of Σ2 boundaries reaching a maximum of 18 %. The study concluded that this increase was a consequence of the finer grain sizes and increased carbide contiguity resulting from the grain inhibition of vanadium. However, in the current work, grain sizes of the standard (13.6 μm) and doped (13.8 μm) samples are similar. Thus, the grain

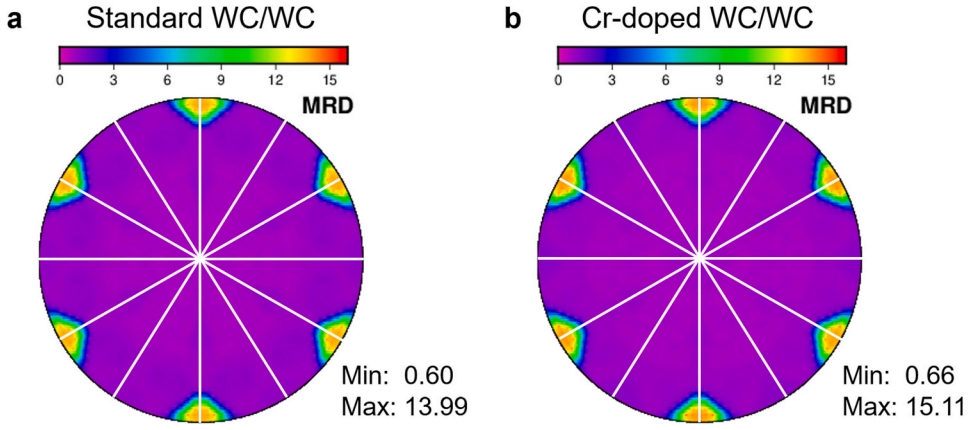

Fig. 3. 90° axis-angle distributions for the standard WC/WC and Cr doped WC/WC boundaries, with minimum and maximum MRD values indicated.

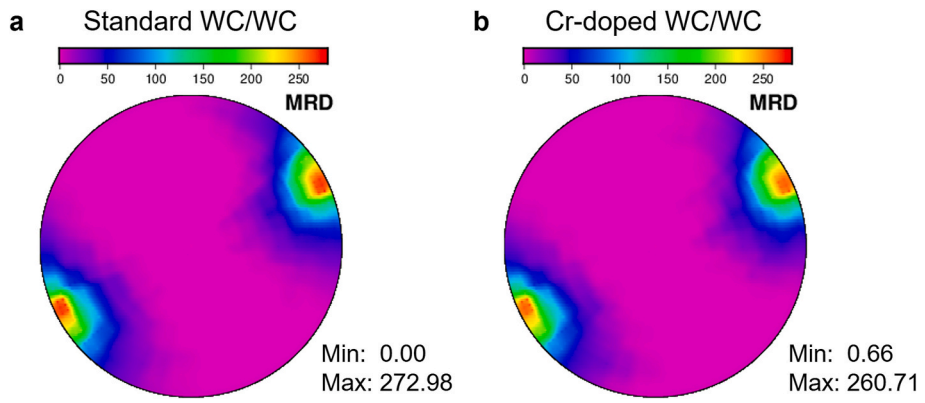

Fig. 4. Σ2 boundary GBCD for the WC/WC boundary segments files for the standard and chromium doped samples, with minimum and maximum MRD values indicated.

Table 1
Area fraction of the Σ2 boundaries determined for the four segment files.

Segment File	Area Fraction of Σ2 Boundaries (%)
Standard WC/WC	12.8
Cr-Doped WC/WC	14.8

growth inhibition can be eliminated as a reason for altering the area fraction of the Σ2 boundaries.

Another study by Yuan et al. investigated the effect of changing the binder in cemented carbide from cobalt to nickel [24]. The authors found that the population of Σ2 boundaries increased when the nickel binder was used instead of the cobalt. This increase was attributed to the change in boundary chemistry of Σ2 boundaries as a result of altering the binder.

Similarly, we propose that chromium doping modifies the boundary chemistry of the Σ2 boundaries and lowers the boundary energy. This in turn is likely to increase the preference for the said boundary and thereby increasing Σ2 boundary area fraction. We also hypothesise that the reduced grain boundary energy alludes to better grain cohesion at the Σ2 boundaries. This is likely to improve the fracture toughness of the Σ2 boundaries. In agreement with this, previous work demonstrated that successful DCB tests could not be performed on the chromium doped sample at Σ2 boundary sites despite performing around 30 tests, where a successful DCB test refers to stable crack growth splitting a Σ2 in a DCB that allows for measurement of fracture energies. In comparison, 1–2 out of 5 DCB tests performed at Σ2 boundaries on the standard sample yielded a stable crack growth ideal for fracture energy measurement [18].

5. Conclusion

In this work, we have examined the effect of chromium doping on the GBCD of WC-Co. We combined the five parameter GBCD analysis with micro-double cantilever splitting experiments. We have found that addition of 1 wt% chromium to a WC-10wt%Co sample increases the boundary area fraction of Σ2 boundaries from 12.8 % to 14.8 %. The increase in boundary fraction suggests a reduction in the Σ2 boundary energy probably caused by an alteration in the boundary chemistry because of chromium doping. This is further supported by circumstantial evidence that Σ2 boundary were un-splitable during the micro-double cantilever splitting tests. This suggests an improved cohesion for the Σ2 boundaries which in turn is likely to improve the fracture toughness of WC-Co given that Σ2 boundaries are the most abundant

Table 2
Experimental parameters used for GBCD analysis of various WC-Co samples in the literature.

Parameters	Literature					In-house Samples in this work	
	Kim and Rohrer, 2004 [23]	Kim et al., 2008 [9]	Yuan, 2013 [11]	Yuan et al., 2013 [13]	Yuan et al., 2014 [20]		
Synthesis Method	Liquid Phase Sintering 1400 °C 45 min	Liquid Phase Sintering 1400–1600 °C 45 min	Sinter-HIP 1500 °C (6 MPa Ar) Duration adjusted for grain size	Sinter-HIP (6 MPa Ar) 1500 °C 30 min / SPS 1200 °C (50 MPa) 5 min	Sinter-HIP 1500 °C 60 min	Vacuum Sintered 1500 °C 60 min	
Cobalt Content (wt%)	6	7–20	Unknown	6 8 10	8	10	10
Chromium Content (wt %)	–	–	–	– – –	–	0	1
Grain Size (μm)	~6	1.4–5.3	0.5 1 2	1	1	13.6	13.8
Step size (μm)	1		0.1	0.1	0.08	0.42	
Fraction of Σ13 boundaries (%)	3	2–3	1.1–2.8	Unknown	Unknown	0.00734	0.00549
Fraction of Σ2 twist boundaries (%)	11	11–14	6.2–10.4	Unknown	10.6–12.7	12.8	14.8
Number of Segments Analysed	$1.56*10^4$	$2.5*10^5$	$1.8*10^5$	Unknown	$2*10^5$	$6.1*10^4$	
EBSD cleaning protocol	Neighbour orientation correlation (NOC) (level 5)	Grain dilation	Unknown	Unknown	Grain dilation (min. Grain size 4 px) + NOC	Grain dilation (min. Grain size 200 px)	

boundary type in WC-Co.

To conclude, this study provides insights into the impact of chromium doping on the grain boundary character distribution (GBCD) and fracture behaviour of WC-Co cemented carbides, a material critical for applications requiring high durability, such as cutting tools and mining equipment. By demonstrating that chromium addition increases the fraction of Σ2 boundaries and potentially enhances grain boundary behaviour, our findings contribute to the development of tougher, more reliable materials that can withstand extreme conditions.

The key conclusions include:

1. When all processing parameters are kept constant for samples of WC-Co cemented carbides, an addition of chromium appears to increase the area fraction of Σ2 grain boundaries.
2. Increase in the Σ2 boundaries with the addition of chromium indicates a lowering of grain boundary energy, which correlates to evidence from previous DCB splitting tests.

Funding sources

This work was supported by Seco Tools AB; and EPSRC [grant numbers P006566, EP/X034968/1, EP/V007661/1].

CRediT authorship contribution statement

Max Emmanuel: Writing – original draft, Methodology, Investigation, Data curation. **Zhuoqi Lucas Li:** Writing – review & editing, Methodology, Formal analysis. **Harry Heptinstall:** Writing – review & editing, Methodology, Formal analysis. **Oriol Gavalda-Diaz:** Writing – review & editing. **Rachid M'saoubi:** Resources, Project administration. **Tomas Persson:** Project administration. **Susanne Norgren:** Resources. **Thomas Benjamin Britton:** Writing – review & editing, Software, Methodology. **Finn Giuliani:** Writing – review & editing, Supervision, Project administration, Methodology, Funding acquisition, Conceptualization. **Katharina Marquardt:** Writing – review & editing, Supervision, Project administration, Methodology, Funding acquisition, Conceptualization.

Declaration of competing interest

The authors declare that they have no known competing financial interests or personal relationships that could have appeared to influence the work reported in this paper.

Appendix A. Supplementary data

Supplementary data to this article can be found online at https://doi.org/10.1016/j.ijrmhm.2024.106954.

Data availability

Data will be made available on request.

References

[1] G.S. Rohrer, et al., The distribution of internal interfaces in polycrystals, Int. J. Mater. Res. Adv. Techn. 95 (4) (2004).
[2] Tungsten carbide market size, share, and trends analysis report by (cemented carbide, coating, alloy) by industry verticals (aerospace and defense, automotive, mining and construction, electronics, medical, sports) based on region, and segment forecasts, 2022.
[3] K. Mingard, et al., In situ observation of crack growth in a WC-co hardmetal and characterisation of crack growth morphologies by EBSD, Int. J. Refract. Met. Hard Mater. 36 (2013) 136–142.
[4] D.M. Saylor, A. Morawiec, G.S. Rohrer, Distribution of grain boundaries in magnesia as a function of five macroscopic parameters, Acta Mater. 51 (13) (2003) 3663–3674.
[5] R.P. Heilbronner, C. Pauli, Integrated spatial and orientation analysis of quartz c-axes by computer-aided microscopy, J. Struct. Geol. 15 (3–5) (1993) 369–382.
[6] D. Rowenhorst, G. Spanos, Crystallographic and morphological analysis by combining EBSD and serial sectioning, Microsc. Microanal. 13 (S02) (2007) 934–935.
[7] S.J. Dillon, G.S. Rohrer, Characterization of the grain-boundary character and energy distributions of yttria using automated serial sectioning and EBSD in the FIB, J. Am. Ceram. Soc. 92 (7) (2009) 1580–1585.
[8] J. Han, V. Vitek, D.J. Srolovitz, Grain-boundary metastability and its statistical properties, Acta Mater. 104 (2016) 259–273.
[9] C.S. Kim, T.R. Massa, G.S. Rohrer, Interface character distributions in WC–co composites, J. Am. Ceram. Soc. 91 (3) (2008) 996–1001.
[10] X. Yuan, Grain boundary character distributions of sigma2 boundaries in WC–co composites with different cobalt volume fractions, Ceram. Int. 40 (1) (2014) 1873–1878.
[11] X. Yuan, Grain boundary character distributions of coincidence site lattice boundaries in WC-co composites with different WC grain sizes, J. Alloys Compd. 579 (2013) 622–627.
[12] X. Yuan, et al., Characterization and comparison of grain boundary character distributions in cemented carbides with different binder phases, Comput. Mater. Sci. 93 (2014) 144–150.
[13] X. Yuan, et al., Effect of densification mechanism on the Σ2 grain boundary plane distribution in WC–co composites, Mater. Lett. 92 (2013) 86–89.
[14] F. Papillon, G.S. Rohrer, P. Wynblatt, Effect of segregating impurities on the grain-boundary character distribution of magnesium oxide, J. Am. Ceram. Soc. 92 (12) (2009) 3044–3051.
[15] S.A. Bojarski, et al., Influence of Y and La additions on grain growth and the grain-boundary character distribution of alumina, J. Am. Ceram. Soc. 97 (2) (2014) 622–630.
[16] S. Tsurekawa, et al., Improvement of oxidation resistance and oxidation-induced embrittlement by controlling grain boundary microstructure in silicon carbides with different dopants, Mater. Trans. 45 (7) (2004) 2128–2136.
[17] X. Liu, et al., Low-energy grain boundaries in WC-co cemented carbides, Acta Mater. 175 (2019) 171–181.
[18] M. Emmanuel, et al., Fracture energy measurement of prismatic plane and Σ2 boundary in cemented carbide, JOM 73 (6) (2021) 1589–1596.
[19] K. Marquardt, et al., The most frequent interfaces in olivine aggregates: the GBCD and its importance for grain boundary related processes, Contrib. Mineral. Petrol. 170 (2015) 1–17.
[20] X. Yuan, et al., Effect of plastic deformation on the Σ2 grain boundary plane distribution in WC–co cemented carbides, Int. J. Refract. Met. Hard Mater. 47 (2014) 38–43.
[21] J. Li, et al., The Σ= 2 and Σ= 13a grain boundary distributions in cemented tungsten carbides with/without metallic binders, Mater. Charact. 173 (2021) 110872.
[22] K. Marquardt, et al., Quantitative electron backscatter diffraction (EBSD) data analyses using the dictionary indexing (DI) approach: overcoming indexing difficulties on geological materials, Am. Mineral. 102 (9) (2017) 1843–1855.
[23] C.-S. Kim, G.S. Rohrer, Geometric and crystallographic characterization of WC surfaces and grain boundaries in WC-co composites, Interf. Sci. 12 (2004) 19–27.
[24] X. Yuan, Effect of different binder phases on the Σ2 grain boundary plane distribution in cemented carbides, J. Superhard Mater. 41 (4) (2019) 229–236.